ISIJ International, Vol. 45 (2005), No. 12, pp. 1838–1847

A Mathematical Model to Study Liquid Inclusion Behavior at the Steel–Slag Interface

J. STRANDH, K. NAKAJIMA, R. ERIKSSON and P. JÖNSSON

Division of Applied Process Metallurgy, KTH, SE-100 44 Stockholm, Sweden.

(*Received on May 17, 2005; accepted on August 30, 2005*)

The separation of non-metallic inclusions at the interface between the steel and the slag in the ladle, tundish and mold is an essential part of the production of clean steel. It is therefore, of great importance to have a deep understanding of the phenomena controlling the transfer of inclusions from the steel to the slag layer. In this work a mathematical model, derived from the equation of particle motion, have been used to study the transfer of liquid inclusions to slags. The effects of the drag, added mass, buoyancy and rebound force on the inclusion transfer are considered. The model relies, to a great extent, on the availability of accurate information of the magnitude of a number of physical properties of the involved phases. Among those properties, the interfacial tension between the phases and the slag viscosity were found to be the most critical. Due to the fact that the availability of experimentally obtained high-temperature physical property data, relevant to the industrial conditions, is scarce in the literature several different model descriptions have been used in this work to estimate these properties. The mathematical model has been used to investigate the separation of liquid non-metallic inclusions, of different size and composition, to a number of different industrial ladle slag compositions.

KEY WORDS: mathematical model; physical properties; non-metallic inclusions; steel making.

1. Introduction

The separation of solid and liquid inclusions at the interface between the steel and the slag in the ladle as well as in the tundish and mold is controlled by interfacial phenomena in the steel–slag-inclusion system. Knowledge of how the interfacial properties governing the inclusion transfer can be controlled in a desirable direction is important in the steel making process. For optimal inclusion removal at a steel–slag interface, good separation of the inclusions to the slag, high dissolution and prevention of reoxidation are important criteria that have to be fulfilled.

Apart from a deepened conceptual understanding of the phenomena of liquid inclusion separation at the interface between steel and slag, it would also be an advantage to have a mathematical model describing the inclusion separation. In the literature there have, over the years, been several attempts to model the growth and removal of inclusions in different metallurgical reactors. Most of these models have assumed that all inclusions reaching the interface between the steel and the slag would be separated from the steel. This approach is not only physically unsound, it might also produce an over estimation of the removal rate of inclusions at the interface between steel and slag. Examples of inclusion growth and removal models in the literature that utilizes this praxis can be for example found in the works of Linder,[1] Hallberg *et al.*[2] and Miki *et al.*[3] This present work aims at the development of a model describing the separation of liquid inclusions to the slag, based on physically sound assumptions. This new model could be, together with the model of the separation of solid inclusions previously described by Nakajima[4] and Strandh *et al.*,[5] used to study the fundamentals of separation of liquid inclusions as well as be used as boundary condition in models describing the growth and removal in various metallurgical reactors.

In this work, a mathematical model for the separation of drops/liquid inclusions in a stagnant fluid have been used to study the separation of liquid inclusions as they have reached the steel–slag interface. The inclusion is assumed to have reached the interface with the flow field with a terminal velocity from the buoyancy force and the fluid dynamic drag. Two modes of inclusion transfer are predicted by the model, one where a steel film is formed between the inclusion and the slag and one without steel film formation. In the model description, the formation of the steel film is determined by the magnitude of the inclusion Reynolds number. The main focus of this work has been to study how liquid inclusions, 50 wt%Al_2O_3–50 wt%CaO and others, behave at the steel–slag interface when no steel film is formed.

The paper is structured in a way where the mathematical model describing the behavior of a spherical liquid inclusion at the steel–slag interface is first outlined in great detail. This is followed by a parameter sensitivity study in order to determine the influence of the model parameters on the predictions of the inclusion transfer. In the same section, the relevant high temperature physical property data available through measurements and model descriptions in the literature are carefully examined. Finally, it is exempli-

fied how the model can be used to study inclusion transfer for industrial conditions, which is done using steel and slag compositions gathered at two steel plants. The results from the application of industrial conditions to the mathematical model are thereafter presented and discussed.

2. Mathematical Model of Liquid Inclusion Behavior at the Steel–Slag Interface

Hadamard and Rybczynski[6] both derived analytical expressions for the stream function for bubbles, drops and particles moving relative to a fluid of infinite extent, with the assumption that the stream flow at large distances from the sphere is expressed as:

$$\frac{\psi}{r^2} \to -\frac{U}{2}\sin^2\theta \quad \text{as } r \to \infty \qquad \text{.....(1)}$$

Then the stream function for slow viscous flow past a sphere is defined in spherical coordinates as:

$$\psi = -\frac{U}{2}r^2\sin^2\theta\left[1-\frac{R_I}{r}\left(\frac{2+3\kappa}{2(1+\kappa)}\right)+\frac{R_I^3}{r^3}\left(\frac{\kappa}{2(1+\kappa)}\right)\right] \qquad \text{.....(2)}$$

where $\kappa=\mu_I/\mu_M$, μ_I is the inclusion viscosity, μ_M is the viscosity of the metal, R_I is the radius of the liquid spherical inclusion, $U=dZ/dt$ is the velocity of the steel flow, Z is the displacement of the inclusion from its original position and r and θ is the distance from the center of the inclusion in the r- and θ-direction respectively. The first term in Eq. (2) comes from the assumption of a uniform flow, the second and third term is due to continuous velocities in the r- and θ-direction at the interface and because no exchange between the phases are assumed to occur.

In this work, a generalized model to describe the liquid inclusion behavior at the liquid steel–slag interface for low and medium Reynolds number was developed. Here, the inclusion is assumed to move towards the interface and the fluid (liquid steel) is assumed to have zero velocity far away from the inclusion. This means that Ψ/r^2 in the above assumption, Eq. (1), should tend to zero. Furthermore, the following general assumptions have been made in the formulation of the mathematical model:

- The flow is axisymmetric.
- The liquid inclusion is small, so that the shape can be considered to be spherical (deforms only if inertial terms are significant) with constant volume.
- Creeping flow.
- No chemical reactions between the phases.
- The interfacial tensions are constant.
- The slag phase is completely liquid.
- The interface between steel and slag is flat.
- The inclusion transfer depends on the buoyancy, added mass, drag and rebound force.
- The inclusion has its original position just beneath the slag and when it has moved a distance of $2R_I$ it is assumed to be fully separated to the slag.

The stream function for a small liquid inclusion moving in a stagnant metal/steel bath can be written as:

$$\psi = -\frac{U}{2}r^2\sin^2\theta\left[-\frac{R_I}{r}\left(\frac{2+3\kappa}{2(1+\kappa)}\right)+\frac{R_I^3}{r^3}\left(\frac{\kappa}{2(1+\kappa)}\right)\right] \qquad \text{.....(3)}$$

In order to simplify Eq. (3), the following variables are introduced:

$$A = \frac{2+3\kappa}{2(1+\kappa)} \qquad \text{.....(4)}$$

and

$$B = \frac{\kappa}{2(1+\kappa)} \qquad \text{.....(5)}$$

Note that for a particle $\kappa\to\infty$, since the inclusion viscosity is much bigger than the metal viscosity, and for a gas bubble $\kappa\to0$, since the viscosity of the gas bubble is much smaller than the metal viscosity. Then Eq. (3) can be rewritten as:

$$\psi = -\frac{U}{2}r^2\sin^2\theta\left[-\frac{R_I}{r}A+\frac{R_I^3}{r^3}B\right] \qquad \text{.....(6)}$$

From Eq. (6), the velocities v_θ and v_r for the inclusion can be determined as well as the normal and tangential stress, and drag coefficients. When the velocities, the shear stress and the additional drag components from the deviatoric normal stress are known, the continuity of normal stresses at the interface, R_I+S, where $R_I \gg S$, and the total drag coefficient can be determined for a liquid spherical inclusion in a stagnant fluid. Since the variation of the slag pressure P_{Slag} near the interface is small during the deformation of the interface due to the small size of the inclusion and Eq. (6), P_{Slag} equals P_{Metal}. The continuity of normal stress across the steel film-slag interface is then given by:

$$P_{Film}-P_{Slag} \cong P_{Film}-P_{Metal} = \frac{2\sigma_{MS}}{R_I+S} - 2\mu_S\left.\frac{\partial v_r}{\partial r}\right|_{r=R_I+S}$$
$$= \frac{2\sigma_{MS}}{R_I+S} + \frac{dZ}{dt}2\mu_S\left[\frac{A}{R_I+2S}-\frac{3B}{R_I+4S}\right]\cos\theta \qquad \text{.....(7)}$$

where P_{Film} is the steel film pressure, μ_S is the slag viscosity, σ_{MS} is the interfacial tension between the metal and the slag and S is the steel film thickness.

The total drag coefficient becomes:

$$C_d = \frac{8}{\mathrm{Re}}\frac{(2+3\kappa)}{(1+\kappa)} \qquad \text{.....(8)}$$

where Re is the inclusion Reynolds number defined as:

$$\mathrm{Re} = \frac{2\rho_M u_\infty R_I}{\mu_M} \qquad \text{.....(9)}$$

where ρ_M is the density of the metal and u_∞ is the terminal velocity, which the inclusion is assumed to have as it reaches the interface given by:

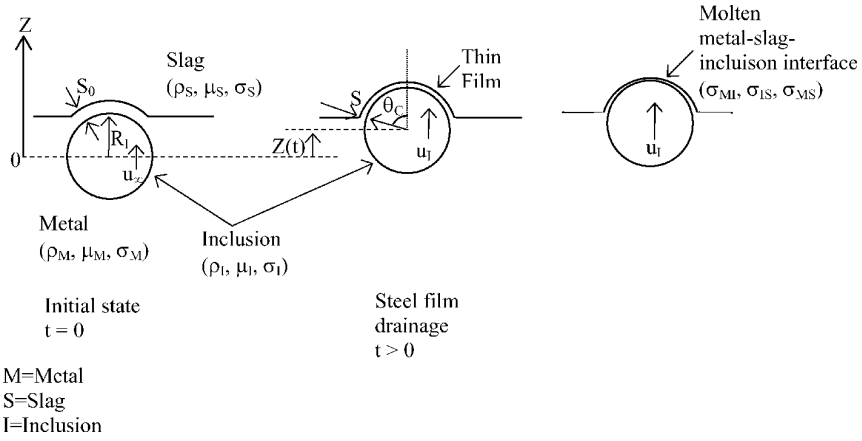

Fig. 1. A schematic description of the liquid inclusion transfer at the steel–slag interface in the steel film case.

$$u_\infty = \frac{2}{3} R_I^2 (\rho_M - \rho_I) \frac{g}{\mu_M} \left(\frac{1+\kappa}{2+3\kappa} \right) \quad \text{.....(10)}$$

where ρ_I is the inclusion density.

2.1. Case with a Film around the Inclusion

As in the model for solid inclusions presented earlier,[4] the steel film formation is considered to occur when Re≥1, as visualized in **Fig. 1**. The forces acting on the inclusion are the drag, the added mass, the buoyancy, and the rebound force.

The physical meaning of steel film formation according to Reynolds number is considered as follows: In the system a spherical particle (solid or liquid) with radius R_I is moving relative to a fluid of infinite extent at a velocity, U. The region affected by the moving particle has the boundary of a paraboloid, expressed as:

$$k(r-x)=c \quad \text{.....(11)}$$

where r is the radius of the paraboloid, x is the displacement of the paraboloid from the centre of the particle and c is a constant equal to 1. Inside the boundary a wake exists between the particle and the paraboloid boundary. The distance between the centre of the particle and the front of the boundary, δ, is given by[7]:

$$\delta = \frac{c}{2k} \quad \text{.....(12)}$$

where

$$k = \frac{U}{2\mu} \quad \text{.....(13)}$$

and μ is the kinematic viscosity.

The affected region by the particle increases with increasing kinematic viscosity. When the wake can be formed and the particle can move with the surrounding fluid, the space (film thickness), S, can be described as:

$$S=(\delta-a) \quad \text{.....(14)}$$

and can be approximately defined as a.

Substituting $\delta=2a$ in Eq. (12), the following is obtained:

$$\mathrm{Re} = \frac{2aU}{\mu} = 1 \quad \text{.....(15)}$$

Thus, Reynolds number is sufficiently low for no film formation at the rear of the particle. It is then considered that the order of the film thickness might be given as the magnitude of the space, S. Actually the steel film formation due to Reynolds number is fuzzy. The real and actual value of Re is between 1 and 2.

The rebound force is obtained by integrating the continuity equation for normal stresses, Eq. (7), according to the following:

$$F_r = -\int_0^{\theta_C} (P_{Film} - P_{Metal}) \cos\theta \cdot 2\pi R_I \sin\theta \cdot R_I d\theta$$

$$= -4\pi R_I^2 \left[\frac{\sigma_{MS}}{2(R_I+S)} \sin^2\theta_C + \frac{dZ}{dt} \frac{\mu_S}{3} \left(\frac{A}{R_I+2S} - \frac{3B}{R_I+4S} \right) (1-\cos^3\theta_C) \right] \quad \text{...(16)}$$

Here $\sin^2\theta_C=(2R_I+S-Z)(S+Z)/(R_I+S)^2$ and $\cos\theta_C=(R_I-Z)/(R_I+S)$ are obtained from inspection of the geometry in Fig. 1. The angle θ_C ranging from 0 to π, is the critical angle from the symmetry axes (dotted line) in Fig. 1 to the steel film–slag-inclusion interface. If θ_C is equal to 0, there is no contact of the inclusion with steel film to the slag and if θ_C is equal to π the inclusion is fully separated to the steel.

The drag force, the added mass force and the buoyancy force are expressed as:

$$F_d = 4\pi R_I \mu_M A \frac{dZ}{dt} \quad \text{.....(17)}$$

$$F_f = \frac{2}{3} \pi R_I^3 \rho_M \frac{d^2Z}{dt^2} \quad \text{.....(18)}$$

and

$$F_b = \frac{4}{3} \pi R_I^3 (\rho_M - \rho_I) g \quad \text{.....(19)}$$

The equation of motion is given by:

$$F_a + F_f = F_b - F_d - F_r \quad \text{.....(20)}$$

where F_a is the force from the acceleration of the inclusion given as:

$$F_a = ma = \frac{4}{3}\pi R_I^3 \rho_I \frac{d^2Z}{dt^2} \quad \text{.....(21)}$$

Although the buoyancy force is always acting upwards, the rebound force, the added mass force and the drag force can act both upwards and downwards depending on the interfacial properties of the system of interest. If the equations for the forces are put into Eq. (20) and some rearrangements are done, the following equation is obtained (For simplicity we make the forces dimensionless to obtain an equation that is easier to solve.):

$$\frac{d^2Z^*}{dt^{*2}} = \frac{2(\rho_M-\rho_I)}{(\rho_M+2\rho_I)} - \frac{3\sigma_{MS}}{R_I^2 g(\rho_M+2\rho_I)} \frac{(2+S^*-Z^*)(S^*+Z^*)}{(1+S^*)^2} - \frac{2\mu_S}{\sqrt{R_I^3 g}(\rho_M+2\rho_I)} \left(\frac{A}{1+2S^*} - \frac{3B}{1+4S^*}\right) \times \left[1-\left(\frac{1-Z^*}{1+S^*}\right)^3\right] \frac{dZ^*}{dt^*} - \frac{6\mu_M A}{R_I^2 g(\rho_M+2\rho_I)} \frac{dZ^*}{dt^*} \quad \text{....(22)}$$

where the dimensionless displacement, steel film thickness, time, velocity and acceleration are expressed as follows:

$$Z^* = \frac{Z}{R_I} \quad \text{.....(23)}$$

$$S^* = \frac{S}{R_I} \quad \text{.....(24)}$$

$$t^* = t\sqrt{\frac{g}{R_I}} \quad \text{.....(25)}$$

$$\frac{dZ^*}{dt^*} = \frac{1}{\sqrt{R_I g}} \frac{dZ}{dt} \quad \text{.....(26)}$$

and

$$\frac{d^2Z^*}{dt^{*2}} = \frac{1}{g}\frac{d^2Z}{dt^2} \quad \text{.....(27)}$$

In order to simplify Eq. (22) the following variables are introduced:

$$C = \frac{\sigma_{MS}}{R_I^2 g(\rho_M+2\rho_I)} \quad \text{.....(28)}$$

$$D(Z^*,S^*) = \frac{(2+S^*-Z^*)(S^*+Z^*)}{(1+S^*)^3} \quad \text{.....(29)}$$

$$E = \frac{\sqrt{R_I^3 g}(\rho_M+2\rho_I)}{\mu_M} \quad \text{.....(30)}$$

$$F = \frac{\sqrt{R_I^3 g}(\rho_M+2\rho_I)}{\mu_S} \quad \text{.....(31)}$$

and

$$G(Z^*,S^*) = \left(\frac{A}{1+2S^*} - \frac{3B}{1+4S^*}\right)\left[1-\left(\frac{1-Z^*}{1+S^*}\right)^3\right] \quad \text{....(32)}$$

After the introduction of these simplifications Eq. (22) can be written as:

$$\frac{d^2Z^*}{dt^{*2}} = \frac{2(\rho_M-\rho_I)}{(\rho_M+2\rho_I)} - 3C\cdot D(Z^*,S^*) - \frac{2}{F}G(Z^*,S^*)\frac{dZ^*}{dt^*} - \frac{6A}{E}\frac{dZ^*}{dt^*} \quad \text{....(33)}$$

The equation for the drainage of the steel film is obtained from the expression for the film surface area, δ, where

$$\delta = \int_0^{\theta_C} (2\pi R_I \sin\theta) R_I d\theta = -2\pi R_I^2(\cos\theta_C - 1) = 2\pi R_I^2 \frac{S+Z}{R_I+S} \quad \text{.....(34)}$$

Continuity of the film flow is expressed as:

$$S\delta - U(2\pi R_I \sin\theta_C)Sdt = (S+dS)(\delta+d\delta) \quad \text{.....(35)}$$

and the film flow-out velocity is given as:

$$U = -\frac{1}{r\sin\theta}\frac{d\psi}{dr} = -\frac{dZ}{dt}\frac{1+2\kappa}{2(1+\kappa)}\sin\theta_C \quad \text{.....(36)}$$

With the above expression inserted into Eq. (35) one obtains:

$$S\delta - \frac{dZ}{dt}(Q\cdot\sin\theta_C)Sdt = (S+dS)(\delta+d\delta) \quad \text{.....(37)}$$

where

$$Q = \frac{1+2\kappa}{2(1+\kappa)} \quad \text{.....(38)}$$

Assuming that the inclusion radius is much bigger than the film thickness, $R_I \gg S$, and neglecting all second order terms in Eq. (37), the steel film drainage per unit time in dimensionless variables is given as:

$$\frac{dS^*}{dt^*} = -Q\frac{dZ^*}{dt^*}\frac{(2-Z^*)(S^*+Z^*)S^*}{2S^*+Z^*} - \frac{S^*}{2S^*+Z^*}\frac{dZ^*}{dt^*} \quad \text{.....(39)}$$

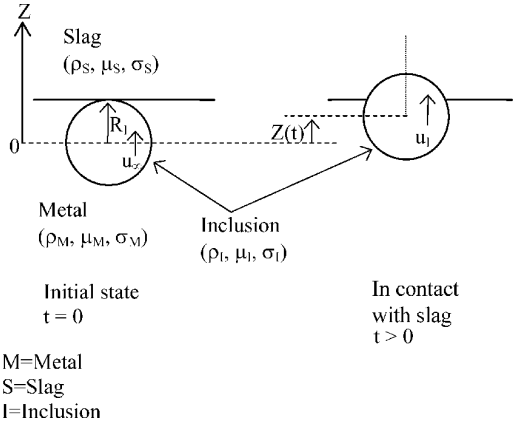

Fig. 2. A schematic description of the liquid inclusion transfer at the steel–slag interface in the non-steel film case.

2.2. Case without a Film around the Inclusion

If the Reynolds number is less than unity, no steel film formation is assumed to occur since the approach of the inclusion towards the interface is slow enough for direct contact with the slag, which is visualized in **Fig. 2**.

The change in interfacial energy by the inclusion transfer across the interface is expressed as:

$$Er = -\pi(2R_I Z - Z^2)\sigma_{MS} + 2\pi R_I Z\sigma_{SI} + 2\pi R_I(2R_I - Z)\sigma_{IM} \quad \text{.....(40)}$$

Similar to the previous discussed case with a film, it is necessary to begin with defining the forces acting on a liquid inclusion. In this case the dimensionless rebound force is defined as:

$$F_r = \frac{dE_r}{dZ} = 2\pi R_I \sigma_{MS} H(Z^*) \quad \text{.....(41)}$$

where

$$H(Z^*) = Z^* - 1 - \cos\theta_{IMS} \quad \text{.....(42)}$$

and

$$\cos\theta_{IMS} = \frac{\sigma_{IM} - \sigma_{IS}}{\sigma_{MS}} \quad \text{.....(43)}$$

where the term $\cos\theta_{IMS}$ expresses the overall wettability. If $\cos\theta_{IMS} > 0$ the system is said to be wetting and if $\cos\theta_{IMS} < 0$ the system is non-wetting.

The dimensionless drag force is given by:

$$F_d = 4\pi\sqrt{R_I^3 g}\,\mu_S A \cdot I(Z^*)\frac{dZ^*}{dt^*} \quad \text{.....(44)}$$

where

$$I(Z^*) = \left(\frac{\mu_M}{\mu_S} - 1\right)Z^{*2} - 2\left(\frac{\mu_M}{\mu_S} - 1\right)Z^* + \frac{\mu_M}{\mu_S} \quad \text{....(45)}$$

The dimensionless added mass force is given by:

$$F_f = \frac{2}{3}\pi R_I^3 g\rho_S J(Z^*)\frac{d^2Z^*}{dt^{*2}} \quad \text{.....(46)}$$

where

$$J(Z^*) = \frac{1}{4}\left(\frac{\rho_M}{\rho_S} - 1\right)Z^{*3} - \frac{3}{4}\left(\frac{\rho_M}{\rho_S} - 1\right)Z^{*2} + \frac{\rho_M}{\rho_S} \quad \text{...(47)}$$

The dimensionless buoyancy force is described as:

$$F_b = \frac{4}{3}\pi R_I^3 g(J(Z^*)\rho_S - \rho_I) \quad \text{.....(48)}$$

In summary, the equation of motion for the non-film case, in dimensionless form, can be written as:

$$\frac{d^2Z^*}{dt^{*2}} = \frac{2(\rho_S J(Z^*) - \rho_I)}{(\rho_S J(Z^*) + 2\rho_I)} - \frac{3\sigma_{MS}}{R_I^2 g(\rho_S J(Z^*) + 2\rho_I)} H(Z^*) - \frac{6A\mu_S}{\sqrt{R_I^3 g}\,(\rho_S J(Z^*) + 2\rho_I)} I(Z^*)\frac{dZ^*}{dt^*} \quad \text{.....(49)}$$

By solving Eqs. (33) and (39), the displacement of the inclusion and the film thickness can be calculated for case with steel film formation, and by solving Eq. (49) the displacement of the inclusion for the case without steel film formation is calculated.

In the present work, the systems of differential equations were solved using the commercial software MATLAB 6.5.

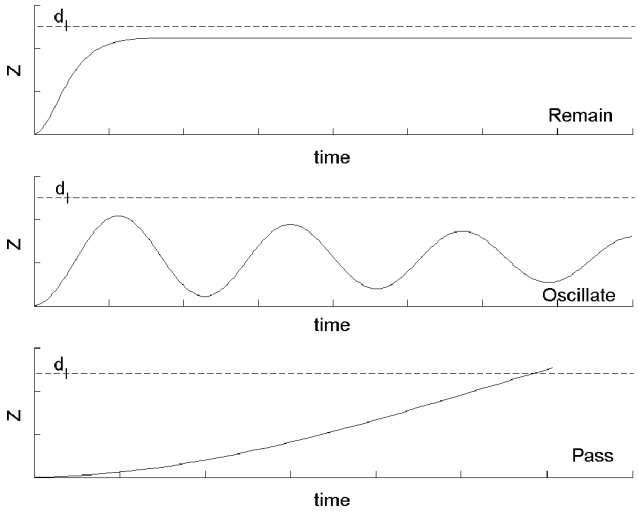

Fig. 3. The three types of inclusion behavior at the steel–slag interface.

3. Liquid Inclusion Behavior Characteristics across the Interface

The solutions of the mathematical model outlined above shows three different types of inclusion behavior at the interface depending on the inclusions size, the velocity of the inclusion and the interfacial properties of the system. In **Fig. 3**, the pass, remain and oscillating modes of inclusion behavior at the interface are illustrated. In the pass mode, the inclusion center has, as mentioned before, traveled a distance of an inclusion diameter and the inclusion is therefore assumed to be fully separated to the slag. If the inclusion experiences the oscillating mode, the inclusion initially rises upwards to a maximum position from which it then descends to a position slightly above the original location. It will then rise again. The oscillation will eventually be damped out and the inclusion will come to rest with the center located at a position beneath the interface. In the remain mode, the inclusion rises, but stays at the interface not separating completely to the slag. To explain the remain state more clearly it should be noted that this is a dynamic model. When the inclusion rises to a maximum position, it is depending on the slag viscosity how far up it can go. Then it tries to move to a neutral position which takes some time. If or when it finds this neutral position, then it can be considered steady state and the acceleration and velocity of the inclusion tends to zero. A relative balance was conducted to control which force that is more dominant in the three types of inclusion behavior. It was found that if the rebound force has the same magnitude for all three cases, then in the remain case $F_r \approx F_d$ making the inclusion stop its upward motion. In the pass case $F_r > F_d$ and in the oscillating case $F_r \gg F_d$.

Both the remain and the oscillating case are harmful in the steel making process, since a steel flow parallel to the

interface can wash these inclusions back into the steel bath. These modes should therefore be avoided. A detailed discussion on the suitable measures and operation conditions to promote the separation of liquid inclusions will be made in a subsequent section. Furthermore, since steel film formation occurs for inclusions larger than 180 μm and in modern steel making processes inclusions of this size is rare, therefore this case has not been studied in this work.

3.1. Parameter Study

The model description outlined in the previous section, rely to a great extent on physical properties and on the accuracy of such. The parameters in the above described mathematical model are the density and viscosity for slag, metal and inclusion, the interfacial tensions between slag–inclusion, metal–inclusion and metal–slag and the radius of the inclusion. In the literature, density (ρ_M, ρ_S, ρ_I), viscosity (μ_M, μ_S, μ_I) and interfacial tension (σ_{MI}, σ_{MS}) data for some of the phases can often be found or at least be calculated by using models. However, it is not possible, to the best knowledge of the authors, to find experimental data of the interfacial tensions between the slag and the liquid inclusion. In addition, it is also difficult to theoretically estimate this physical property, but models do exist. This will be elaborated further in the following.

Girifalco and Good[8] have developed a network parameter model for the estimation of interfacial tension between two phases, originally water and oil. In their model, the interfacial tension is expressed as:

$$\sigma_{ab}=\sigma_a+\sigma_b-2\phi_{ab}\sqrt{\sigma_a\cdot\sigma_b} \quad \text{.....(50)}$$

where the subscripts a and b denotes the two phases, σ_{ab} is the interfacial tension between the two phases a and b, σ_a and σ_b are the surface tension of each phase and finally ϕ_{ab} is the interaction parameter between a and b. The interaction parameter is obtained from a regression analysis of experimental data. If the interaction parameter is close to zero, one says that the attraction between the phases is weak and if the interaction parameter is close to unity the attraction is strong.

Nakajima[9] has also developed a model for the estimation of the surface tension of slags. Since liquid inclusions can be regarded as being microscopic droplets of slags, this model can be used for our purpose. Then in order to calculate the interfacial tension using Eq. (50), the interaction parameter between the slag and the inclusion needs to be known. However, no data for the interaction parameter between two liquid slags have been found reported in the literature and since no measurements of the interfacial tension between two liquid slags could be found, the interaction parameter can not be estimated.

In the light of the above mentioned limitations, a parameter study was made in order to investigate the behavior of the interfacial tension between a liquid inclusion and a liquid slag for different interaction parameters. In **Table 1**, a slag and two liquid inclusions with typical compositions for industrial conditions with the corresponding calculated surface tensions at 1 773 K and 1 873 K using the method proposed by Nakajima[9] are summarized. The result of the interfacial tension between inclusion and slag dependent on the interaction parameter for the liquid inclusions in Table 1 compared with a solid Al_2O_3 inclusion is visualized in **Fig. 4**. Here it is seen that the interfacial tension has its maximum when the interaction between the phases is low, and minimum when the interaction parameter is close to unity. Also, when comparing the composition of the three inclusions it is concluded that the lower inclusion surface tension, the lower interfacial tension between slag and inclusion. The inclusion surface tension is seen to depend on the amount of Al_2O_3. Higher amount of alumina gives a higher inclusion surface tension. Moreover, the temperature does not seem to affect how the interaction parameter influences the interfacial tension.

Now, in order to investigate which of the physical property parameters in the model that have the greatest influence on the inclusion transfer, the 50 wt%Al_2O_3–50 wt%CaO inclusion (Inclusion 2) from Table 1 was chosen. Pure iron containing 0.005 wt% S and 0.0025 wt% O at 1 823 K,

Table 1. The chemical composition and surface tension at 1 773 K and 1 873 K for one slag and two liquid inclusions.

	Chemical composition (wt%)						$\sigma^{9)}$ (N/m) 1773 K	$\sigma^{9)}$ (N/m) 1873 K
	SiO_2	Al_2O_3	CaO	MgO	CaF_2	Na_2O		
Slag[14)]	44.1	6.6	34.6	2.6	4.3	7.8	0.386	0.3864
Inclusion 1 (I1)	2	46	45	7	-	-	0.549	0.542
Inclusion 2 (I2)	-	50	50	-	-	-	0.611	0.602

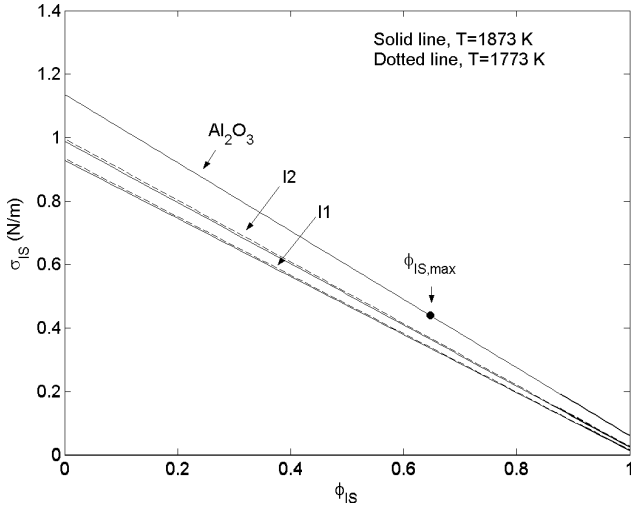

Fig. 4. The effect of the interaction parameter on the interfacial tension between the solid Al_2O_3 inclusion, the liquid inclusions (I1 and I2) and the liquid slag, defined in Table 1, at 1 773 K and 1 873 K.

Table 2. Original calculation conditions.

σ_M[14)] (N/m)	σ_S[14)] (N/m)	σ_I[9)] (N/m)	μ_M[14)] (Pa·s)	μ_S[14)] (Pa·s)	μ_I[10)] (Pa·s)	ρ_M[14)] (kg/m^3)
1.606	0.386	0.606	0.006	0.1998	0.118	7000
ρ_S[14)] (kg/m^3)	ρ_I[13)] (kg/m^3)	σ_{MS}[14)] (N/m)	σ_{MI}[12)] (N/m)	σ_{IS} (N/m)	ϕ_{IS} (-)	T (K)
2543	2814	1.375	1.336	0.508	0.5	1823

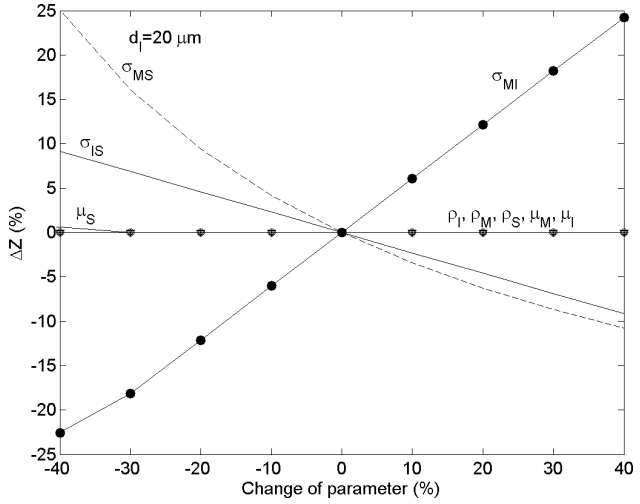

Fig. 5. The influence of the physical properties on the transfer of a 20 μm liquid Al_2O_3–CaO (50/50 wt%) inclusion when changed by ±40%. Note, that the interaction parameter between the inclusion and the slag is here set to 0.5.

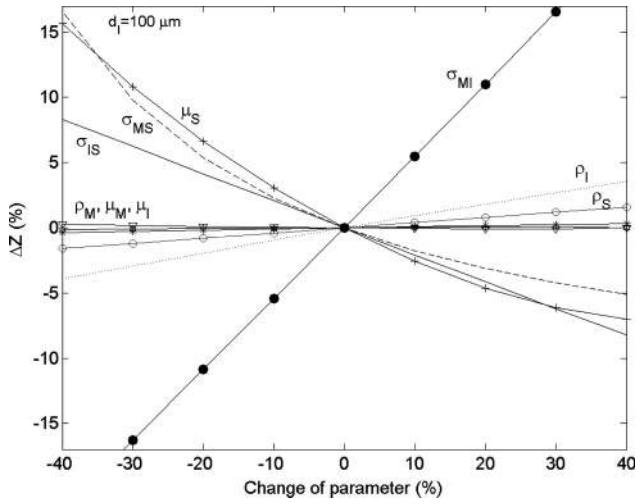

Fig. 6. The influence of each physical property parameter when changed by ±40% on the inclusion displacement for a 100 μm liquid Al_2O_3–CaO (50/50 wt%) inclusion. Note, that the interaction parameter between inclusion and slag is here set to a value of 0.5.

together with a slag containing (44.1 wt%)SiO_2–(6.6 wt%)Al_2O_3–(4.3 wt%)CaF_2–(2.6 wt%)MgO–(34.6 wt%)CaO–(7.8 wt%)Na_2O were selected. Since the interfacial tension between the liquid 50 wt%Al_2O_3–50 wt%CaO inclusion (Inclusion 2) and the liquid slag cannot be found in the literature nor be estimated, the interaction parameter ϕ_{IS} were given the value 0.5. In **Table 2**, the original calculation conditions are summarized for the steel, the slag and the inclusion.

Then each parameter was varied, one at the time, in the range −40 to +40% about its original value given in Table 2. The percentage deviation from the original inclusion displacement was plotted against the change of the parameter in percent, visualized in **Fig. 5** for a 20 μm inclusion and in **Fig. 6** for a 100 μm inclusion. From this parameter study it can be concluded that for a 20 μm liquid 50 wt%Al_2O_3–50 wt%CaO inclusions the interfacial tensions plays an important role in the inclusion transfer to the slag. For a 100 μm inclusions the density of the inclusion as well as

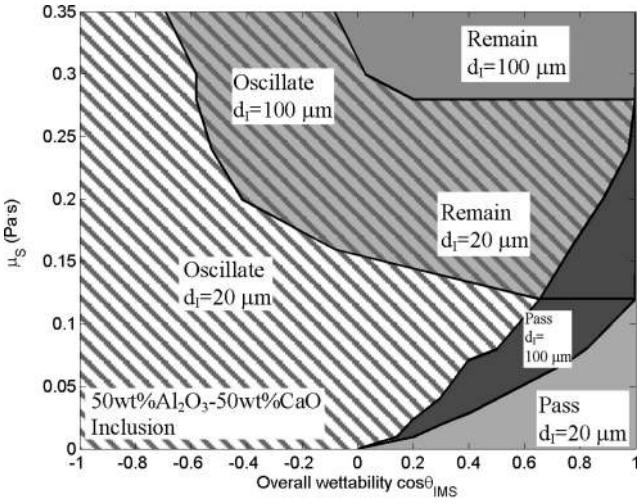

Calculation conditions:

σ_{MS}[14] (N/m)	σ_{MI}[12] (N/m)	ρ_M[14] (kg/m3)	ρ_S[14] (kg/m3)	ρ_I[13] (kg/m3)	μ_M[14] (Pa s)
1.375	1.336	7000	2543	2814	0.006
μ_I[10] (Pa s)	σ_S[14] (N/m)	σ_I[9] (N/m)	σ_M[14] (N/m)	ϕ_{MS}[14]	ϕ_{MI}[12]
0.118	0.386	0.606	1.606	0.392	0.444

Fig. 7. The effect of the slag viscosity and the wettability on the behavior of a liquid Al_2O_3–CaO (50/50 wt%) inclusion.

the viscosity of the slag are also important besides the interfacial tensions and the slag viscosity.

Since the overall wettability is expressed by the interfacial tensions, see Eq. (43), another approach of the parameter study was taken, where the overall wettability and the slag viscosity were varied to investigate the effect on the inclusion behavior at the interface. In **Fig. 7**, the result is illustrated for a 20 μm and a 100 μm liquid 50 wt%Al_2O_3–50 wt%CaO inclusion. Here it is seen that the larger the inclusion is, the larger the pass region is. Moreover, the oscillating region increases with increasing inclusion diameter, which can lead to an increase in the number of inclusions re-entering the steel bath if the conditions are not right. Also, it can be concluded that a high overall wettability and a low slag viscosity is preferable for optimal inclusion transfer. Now, if we return to the results from the investigation of the effect of the interaction parameters (in equation (50)) on the interfacial tension (Fig. 4) between the slag and the inclusion, it can be seen that if the interfacial tension is large, then the overall wettability will be small. This in turn will give an inclusion in the oscillating region. From this point of view, it is also concluded that a high interaction between the phases are desirable in order to obtain good inclusion transfer to the slag.

A comparison between the behaviors of liquid 50 wt%Al_2O_3–50 wt%CaO inclusions with solid Al_2O_3 inclusions from an earlier study[5] is illustrated in **Fig. 8**. According to Fig. 8, solid alumina inclusions have a larger pass region than the liquid 50 wt%Al_2O_3–50 wt%CaO inclusion. This is more obvious for the 100 μm inclusions. From the parameter study illustrated in Fig. 6 it is seen that the inclusion density starts to affect the inclusion transfer to the slag for 100 μm inclusions. This might be the reason why the pass area for the heavier solid alumina inclusion is larger than for the lighter liquid 50 wt%Al_2O_3–50 wt%CaO

inclusion. Also, the oscillating region is larger for the alumina inclusion. Therefore, the conclusion is that solid Al_2O_3 inclusions are easier to separate than the liquid 50 wt%Al_2O_3–50 wt%CaO inclusions to the slag under the current conditions. Moreover, by comparing the parameter studies for the 20 μm solid Al_2O_3 inclusion and the 20 μm liquid 50 wt%Al_2O_3–50 wt%CaO inclusion it is seen that the slag viscosity affects the inclusion displacement more for the solid inclusion than for the liquid inclusion. The shift in the oscillating/remain line between the solid and liquid 20 μm inclusions is probably caused by this.

4. Industrial Conditions

Two steel plants were chosen, to test the applicability of the above described model on liquid 50 wt%Al_2O_3–50 wt%CaO inclusions. One of the steel plants is a tool steel producer and from now designated *PLANT1*. The other steel plant is a wire and bolt steel producer, designated *PLANT2* with two steel grades. In this work, the separation of liquid 50 wt%Al_2O_3–50 wt%CaO inclusions to the slag for two different heats from each plant was studied. The compositions of the steel and the slag for the two plants are summarized in **Table 3** and **Table 4** respectively.

To apply the above described mathematical model for liquid inclusion transfer, in the non-steel film formation mode, to the conditions found in the two steel plants investigated in this study, there are some physical property parameters (ρ_S, ρ_I, ρ_M, μ_S, μ_M, σ_{IS}, σ_{MI} and σ_{MS}) that needs to be determined. Since the results of the parameter study showed that the influence of some of these parameters (σ_{IS}, σ_{MI} and σ_{MS} and μ_S) on the predictions is large, it is crucial to have access to data of high accuracy in order to make reliable predictions. Furthermore, the lack of experimental data for these physical properties, applicable to systems of industrial relevance, leaves us to estimations by using different methods.

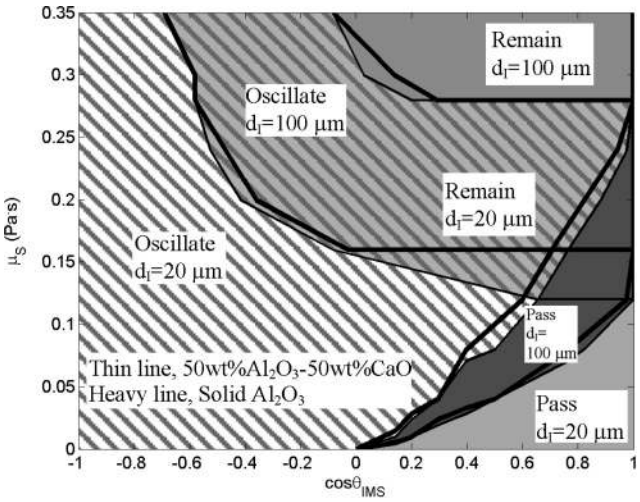

Calculation conditions:

Inclusion	μ_M[14] (Pa s)	μ_S[14] (Pa s)	μ_I[10] (Pa s)	ρ_M[14] (kg/m^3)	ρ_S[14] (kg/m^3)	ρ_I[13] (kg/m^3)	σ_{MS}[14] (N/m)	σ_{MI}[12] (N/m)
Al_2O_3	0.006	0.1998	-	7000	2543	3990	1.375	1.518
50wt%Al_2O_3-50wt%CaO	0.006	0.1998	0.118	7000	2543	2814	1.375	1.336

Fig. 8. Comparison of the transfer behavior of liquid Al_2O_3–CaO (50/50 wt%) and solid Al_2O_3 inclusion with diameters of 20 μm and 100 μm.

The slag viscosity was one of the parameters that earlier was shown to have a large influence on the liquid inclusion transfer to the slag. Experimental data for the slag viscosity in the literature is limited. Therefore, a model by Nakajima[10] based on the network parameter model, originally developed by Iida[11] was used to estimate the viscosity for the industrial slags. The interfacial tensions between metal–inclusion and metal–slag were also determined by a model developed by Nakajima[12] based on the work by Girifalco and Good[8]. Finally, the slag and inclusion density were estimated by using a model developed by Nakajima[13] for the estimation of slag density with an interaction parameter introduced in the model.

No experimental data for the interfacial tension between inclusion-slag and the interaction parameter in Eq. (50) were found in the open literature. In order to make calculations of inclusion transfer, the interaction parameter ϕ_{IS} were investigated for a solid Al_2O_3 inclusion and slags with variable basicity. Here the basicity is defined as the following ratio, Al_2O_3/CaO. The results can be seen in **Table 5**. It

Table 4. The chemical composition of the industrial ladle slags investigated in this study.

	Slag	Description	Slag composition (wt%)			
			CaO	SiO_2	Al_2O_3	MgO
PLANT1,1	A1	Ladle slag	48.2	8.9	32.9	10
PLANT2,1	B1	Ladle slag	47.5	12.5	30	10
PLANT2,2	B2	Ladle slag	40	35	15	10

Table 5. The effect of the slag basicity on the interaction parameter for solid alumina inclusions.

Al_2O_3	SiO_2	CaO	MgO	ϕ_{IS}	Al_2O_3/CaO
0	45	45	10	0.6904	0
5	40	45	10	0.6977	0.1111
10	35	45	10	0.7057	0.2222
15	30	45	10	0.7143	0.3333
20	25	45	10	0.7238	0.4444
25	20	45	10	0.7341	0.5556
30	15	45	10	0.7453	0.6667
35	10	45	10	0.7575	0.7778
40	5	45	10	0.7709	0.8889
45	0	45	10	0.7855	1

Table 3. Steel composition (wt%) for the two steel plants investigated in this study.

	C	S	Mn	P	Cu	Si	Ca	Ni	B
PLANT1,1	0.4	0.0014	0.39	0.009	0.13	1.14	0.0002	0.14	0.0001
PLANT2,1	0.22	0.010	0.9	-	-	0.08	0.003	-	-
PLANT2,2	0.72	0.008	0.5	-	-	0.22	0.0001	-	-
	V	Ce	Al	Ti	Cr	Sn	Mo	N	Co
PLANT1,1	0.94	0.003	0.02	0.0025	5.12	0.005	1.46	0.009	0.04
PLANT2,1	-	-	0.03	-	0.33	-	-	-	-
PLANT2,2	-	-	0.0005	-	0.05	-	-	-	-

Table 6. Estimation of physical properties of the industrial ladle slags investigated in this study.

Plant	σ_M [9] (N/m)	ρ_M [15] (kg/m^3)	μ_M [14] (Pa·s)	σ_S [9] (N/m)	ρ_S [13] (kg/m^3)	μ_S [10] (Pa·s)	σ_I [9] (N/m)	ρ_I [13] (kg/m^3)	μ_I [10] (Pa·s)
PLANT1,1	1.856	7750	0.006	0.546	2772	0.067	0.606	2718	0.118
PLANT2,1	1.467	7850	0.006	0.539	2755	0.0674	0.606	2718	0.118
PLANT2,2	1.571	7840	0.006	0.468	2660	0.1977	0.606	2718	0.118
Plant	σ_{MS} [12] (N/m)	σ_{MI} [12] (N/m)	σ_{IS} (N/m)	$\cos\theta_{IMS}$ (-)	T (K)				
PLANT1,1	1.458	1.521	0.278*	0.853*	1823				
PLANT2,1	1.191	1.236	0.276*	0.806*	1823				
PLANT2,2	1.361	1.311	0.318**	0.730**	1823				

* ϕ_{IS}=0.76
** ϕ_{IS}=0.71

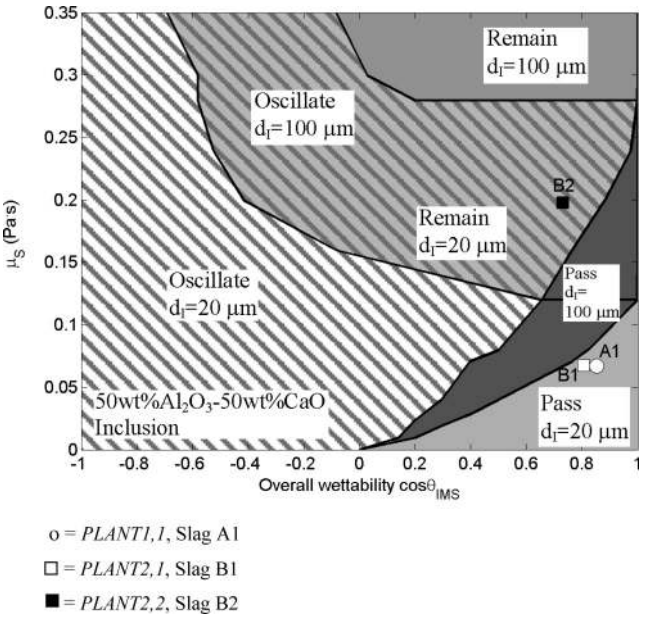

o = *PLANT1,1*, Slag A1
□ = *PLANT2,1*, Slag B1
■ = *PLANT2,2*, Slag B2

Fig. 9. Estimation of the relationship between the slag viscosity and wettability for the conditions in *PLANT1* and *PLANT2*.

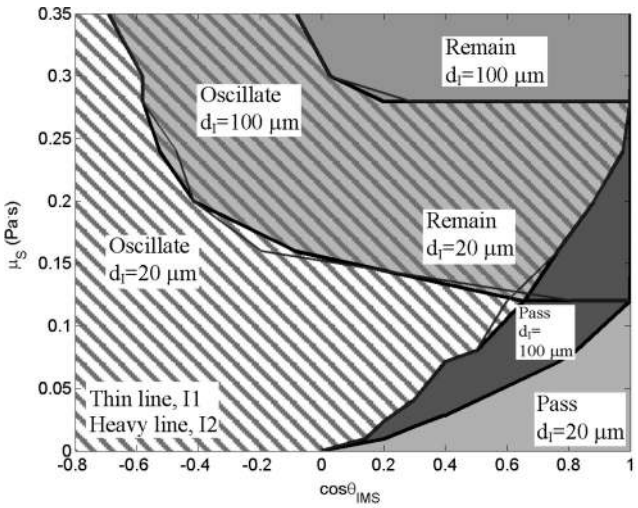

I1=2wt%SiO_2-46wt%Al_2O_3-45wt%CaO-7wt%MgO inclusion
I2=50wt%Al_2O_3-50wt%CaO inclusion

Calculation conditions:

Inclusion	μ_M [14] (Pa·s)	μ_S [14] (Pa·s)	μ_I [10] (Pa·s)	ρ_M [13] (kg/m^3)	ρ_S [14] (kg/m^3)	ρ_I [13] (kg/m^3)	σ_{MS} [14] (N/m)	σ_{MI} [12] (N/m)
I1	0.006	0.1998	0.087	7000	2543	2810	1.375	1.277
I2	0.006	0.1998	0.118	7000	2543	2814	1.375	1.336

Fig. 10. Comparison of the transfer behavior of two liquid inclusions (Table 1) at the steel/slag interface.

can be concluded that the slag basicity has a large influence on the interaction parameter for solid Al_2O_3 inclusions. The larger the slag basicity is, the larger the interaction parameter becomes. Furthermore, in Table 5 the interaction parameter varies little with the slag basicity, only between 0.69–0.78. It can also be seen that for the slags with similar basicity as the industrial slags the interaction parameter for solid alumina inclusions lies between 0.71 (Slag B2)–0.76 (Slag A1 and Slag B1). This limits the magnitude of the interaction parameter. Moreover, since the liquid 50 wt%Al_2O_3–50 wt%CaO inclusion has a surface tension that is less than the surface tension for the pure alumina inclusion, one can suspect that the interfacial tension between the inclusion and slag for the 50 wt%Al_2O_3–50 wt%CaO inclusion will also be less than for the alumina inclusion. Also, the lower interfacial tension between slag and inclusion the higher overall wettability is obtained. The conclusion is therefore that if we use the interaction parameter for the solid alumina inclusion (which is known) then the overall wettability for the industrial slags with a liquid 50 wt%Al_2O_3–50 wt%CaO inclusion and the interaction parameter are slightly larger. The results from the estimation of the physical properties are summarized in **Table 6**.

5. Results and Discussion

After determining the physical properties of the three slags (A1, B1 and B2), the displacement of the liquid 50 wt%Al_2O_3–50 wt%CaO inclusion from its original position was calculated. The interaction parameter, ϕ_{IS}, was set to 0.76 for slag A1 and B1 and to 0.71 for slag B2. The results of these calculations are presented as a function of the slag viscosity and the overall wettability in **Fig. 9**. The changes from remain to pass, from pass to oscillate and from remain to oscillate are in the same figure plotted for a 20 μm inclusion and a 100 μm inclusion. Since the slag basicity in Table 5 only varied between 0.69–0.78, it have been concluded that the influence of the slag bacisity on the displacement of the liquid 50 wt%Al_2O_3–50 wt%CaO inclusion is very small. Thus, no attempt to visualize the influence of the slag bacisity on the inclusion displacement has been made. It can be seen that the best slags for liquid 50 wt%Al_2O_3–50 wt%CaO inclusion transfer is slag A1 of *PLANT1* and slag B1 of *PLANT2*. The low slag viscosity while at the same time the overall wettability is positive is favorable to the separation of the inclusions. For slag B2 in

PLANT2, the slag viscosity should be decreased in order to obtain better inclusion transfer since now neither the 100 μm inclusion nor the 20 μm inclusion pass the steel–slag interface.

5.1. Other Liquid Inclusions

Liquid inclusions with various compositions are often found during the processing of steel. To get an understanding of how the areas of inclusion behavior changes with different inclusions, a similar study as in Sec. 3.1 were made for the liquid 2 wt%SiO_2–45 wt%Al_2O_3–46 wt%CaO–7 wt%MgO inclusion (Inclusion 1) in Table 1. The result was compared with the 50 wt%Al_2O_3–50 wt%CaO inclusion (Inclusion 2), visualized in **Fig. 10**. It can be seen that for Inclusion 1 and Inclusion 2 the areas of remain, pass and oscillate are almost the same. This could be expected since both inclusions have almost the same density and viscosity.

6. Conclusions

A mathematical model has been developed to study liquid inclusion behavior and separation at a steel–slag interface. There are three typical behaviors that an inclusion can adopt as it reaches the interface, it can pass and separate to the slag, remain at the interface, or oscillate. In the two later cases there is a risk that the inclusion which has reached the interface without being separated might follow the steel flow back to the bath causing product defects. The model distinguishes between two different ways of inclusion separation based on the inclusion Reynolds number. One is when a steel film is formed between the inclusion and the slag, and the other is when no film is formed and the inclusion Reynolds number Re$<$1. In this work, steel film formation occurs when the inclusion diameter is roughly 180 μm. Because most of the inclusions found in modern steel grades are less than 180 μm, the non-film case is the most relevant model to use.

The main conclusion is that the described mathematical model can be used to determine the most critical parameters governing the non-metallic inclusion separation to the slag. A parameter study showed that the most important parameters were the interfacial tensions (σ_{MS}, σ_{MI}, σ_{IS}) and the slag viscosity (μ_S). For 100 μm inclusions the inclusion density also affects the inclusion transfer. The combined effect of these parameters showed that the overall wettability should be positive and the slag viscosity should be as low as possible without causing slag entrainment into the steel, in order to get the most favorable inclusion transfer conditions. It should though be mentioned that these parameters are also the most difficult ones to find experimental data for in the literature. Thus, future experiments are needed in order to make the predictions of the inclusion behavior at the steel–slag interface more relevant for the industry.

The model was applied to three industrial slags originating from samples taken from the ladle at two different steel plants. Since the slag compositions used in the two steel plants in this study never have been studied experimentally regarding physical properties such as viscosity and interfacial tension, there is no such experimental data available. Instead, the necessary physical properties were estimated using available models. From this study of industrial conditions, very useful plots can be made, showing the tendency for inclusion transfer across the steel–slag interface. Moreover, it can also illustrate how the slag viscosity and the overall wettability should be modified in order to increase the separation of the liquid inclusions to the slag.

Acknowledgements

The Swedish Steel Producers Association and STEM are acknowledged for financing this work. Furthermore, the helpful comments from the members of the committee JK24046 throughout this work.

Nomenclature

g:	Gravity	(m/s^2)
t:	Time	(s)
t^*:	Dimensionless time	(−)
Z:	Displacement of the inclusion	(m)
$Z(0)$:	Initial position of the inclusion	(m)
S:	Steel film thickness	(m)
$S(0)$:	Initial steel film thickness	(m)
u_∞:	Terminal/initial velocity of the inclusion at t=0	(m/s)
R_I:	Radius of the inclusion	(m)
D_I:	Diameter of the inclusion	(m)
Re:	Reynolds number $= \dfrac{\rho_M u_\infty D_I}{\mu_M}$	(−)
ρ_x:	Density	(kg/m^3)
σ_x:	Surface tension	(N/m)
σ_{xy}:	Interfacial tension	(N/m)
μ_x:	Viscosity	(Pa·s)

Subscripts

S:	Slag
I:	Inclusion
M:	Metal

Superscript

*:	Dimensionless

REFERENCES

1) S. Linder: *Scand. J. Metall.*, **3** (1974), 137.
2) M. Hallberg, P. G. Jönsson, T. L. I. Jonsson and R. Eriksson: *Scand. J. Metall.*, **34** (2005), 41.
3) Y. Miki and B. G. Thomas: *Metall. Mater. Trans. B*, **30B** (1999), 639.
4) K. Nakajima and K. Okamura: Proc. of 4th Int. Conf. on Molten Slags and Fluxes, ISIJ, Tokyo, (1992), 505.
5) J. Strandh, K. Nakajima, R. Eriksson and P. Jönsson: *ISIJ Int.*, **45** (2005), 1597.
6) R. Clift, J. R. Grace and M. E. Weber, Bubbles, Drops and Particles, Academic Press, INC., Boca Raton, FL, (1978), 30.
7) Fluid Mechanics Handbook, 2nd ed., Japan Society of Fluid Mechanics, Tokyo, (1998), 102.
8) L. A. Girifalco and R. J. Good: *J. Phys. Chem.*, **61** (1957), 904.
9) K. Nakajima: *Tetsu-to-Hagané*, **80** (1994), 599.
10) K. Nakajima, H. Mizukami, M. Kawamoto and Z. Morita: *Tetsu-to-Hagané*, **80** (1994), 509.
11) T. Iida, Z. Morita and T. Mizobuchi: 3rd Int. Conf. on Molten Slags and Fluxes, Institute of Metals, London, (1988), 199.
12) K. Nakajima: *Tetsu-to-Hagané*, **80** (1994), 383.
13) K. Nakajima: *Tetsu-to-Hagané*, **80** (1994), 593.
14) K. Nakajima: Ph.D. Thesis, Osaka University, Osaka, Japan (1993).
15) Metals Handbook, Desk edition, American Society for Metals, Metals Park, OH, (1985), 1.